



Contents lists available at ScienceDirect

Journal of the Mechanical Behavior of Biomedical Materials

journal homepage: www.elsevier.com/locate/jmbbm

Effects of repeated biaxial loads on the creep properties of cardinal ligaments



Adwoa Baah-Dwomoh, Raffaella De Vita*

STRETCH Laboratory, 330A Kelly Hall, 325 Stanger Street, Virginia Tech, Blacksburg, VA 24061, United States

ARTICLE INFO

Keywords:

Cardinal ligament
Planar biaxial testing
Digital image correlation
Viscoelasticity
Repeated creep

ABSTRACT

The cardinal ligament (CL) is one of the major pelvic ligaments providing structural support to the vagina/cervix/uterus complex. This ligament has been studied mainly with regards to its important function in the treatment of different diseases such as surgical repair for pelvic organ prolapse and radical hysterectomy for cervical cancer. However, the mechanical properties of the CL have not been fully determined, despite the important *in vivo* supportive role of this ligament within the pelvic floor. To advance our limited knowledge about the elastic and viscoelastic properties of the CL, we conducted three consecutive planar equi-biaxial tests on CL specimens isolated from swine. Specifically, the CL specimens were divided into three groups: specimens in group 1 ($n = 7$) were loaded equi-biaxially to 1 N, specimens in group 2 ($n = 8$) were loaded equi-biaxially to 2 N, and specimens in group 3 ($n = 7$) were loaded equi-biaxially to 3 N. In each group, the equi-biaxial loads of 1 N, 2 N, or 3 N were applied and kept constant for 1200 s three times. The two axial loading directions were selected to be the main *in-vivo* loading direction of the CL and the direction that is perpendicular to it. Using the digital image correlation (DIC) method, the in-plane Lagrangian strains in these two loading directions were measured throughout the tests. The results showed that CL was elastically anisotropic, as statistical differences were found between the mean strains along the two axial loading directions for specimens in group 1, 2, or 3 when the equi-biaxial load reached 1 N, 2 N, or 3 N, respectively. For specimens in group 1 and 2, no statistical differences were detected in the mean normalized strains (or, equivalently, the increase in strain over time) between the two axial loading directions for each creep test. For specimens in group 3, some differences were noted but, by the end of the 3rd creep test, there were no statistical differences in the mean normalized strains between the two axial loading directions. These findings indicated that the increase in strain over time by the end of the 3rd creep test were comparable along these directions. The greatest mean normalized strain (or, equivalently, the largest increase in strain over time) was measured at the end of the 1st creep test ($t = 1200$ s), regardless of the equi-biaxial load magnitude or loading direction. Mean normalized strains during the 2nd and 3rd creep tests ($t = 100, 600, \text{ and } 1200$ s), along each loading direction, were not statistically different. Isochronal data collected at 1 N, 2 N, or 3 N equi-biaxial loads indicated that the CL may be a nonlinear viscoelastic material. Overall, this experimental study offers new knowledge of the mechanical properties of the CL that can guide the development of better treatment methods such as surgical reconstruction for pelvic organ prolapse and radical hysterectomy for cervical cancer.

1. Introduction

Pelvic floor disorders (PFDs), such as urinary incontinence, fecal incontinence, and pelvic organ prolapse (POP) are a growing component of women's health issues in the United States. It has been estimated that in 2010 over 28 million women had at least one PFD and this number is expected to increase to 44 million by 2050 (Wu et al., 2009). In particular, POP, the descent of a pelvic organ from its normal place towards the vaginal walls and into the vaginal cavity, is one of the most

prevalent forms of PFDs. As of 2010, it is estimated that POP affects 3.3 million women in the United States, annually (Price et al., 2014). The onset of POP can be attributed to several factors, with the most common being age, labor, parity, menopause, and weight gain (MacLennan et al., 2000; Hendrix et al., 2002; Nygaard et al., 2008). For mild cases of POP, lifestyle changes such as a change in diet and exercise or muscle strengthening exercises such as Kegel exercises can help alleviate some of the symptoms. For more severe or extreme cases, the recommended course of treatment for the most common type of POP, the uterine

* Corresponding author.

E-mail address: devita@vt.edu (R. De Vita).

URL: <http://www.beam.vt.edu/devita> (R. De Vita).

<http://dx.doi.org/10.1016/j.jmbbm.2017.05.038>

Received 21 December 2016; Received in revised form 22 May 2017; Accepted 30 May 2017

Available online 31 May 2017

1751-6161/ © 2017 Elsevier Ltd. All rights reserved.

prolapse, is typically a pelvic reconstructive surgery. The number of women who will undergo surgery to treat POP continues to dramatically increase, and it has been estimated that this number will increase from 166,000 in 2010 to approximately 250,000 in 2050 (Wu et al., 2011).

Traditionally, native tissue repairs have been adopted to treat POP but mesh augmented repairs have become more common over the past years. However, many women experienced adverse side effects to mesh augmented procedures, such as pain, mesh erosion, dyspareunia, and recurrence of POP. A comprehensive study by Maher et al., who collected data on surgical management of POP of approximately 6000 women, found that 14% of patients who received a transvaginal mesh experienced some form of POP recurrence (Maher et al., 2011). The study also found that 18% of patients who received a transvaginal mesh experienced mesh erosion and 11% of patients underwent reoperation. Surgical meshes used for PFDs were developed in the 1950s initially to treat abdominal hernia repairs and, due to their success, in the 1970s gynecologists started using these abdominal meshes for repair of POP (Ellington and Richter, 2013). However, women experienced many of the complications outlined above and these were, most likely, triggered by the mismatch in properties between the native tissue and the synthetic mesh.

Damage to pelvic supportive ligaments, such as the uterosacral ligament (USL) and the cardinal ligament (CL), contributes significantly to the development of PFDs (DeLancey, 1992; Wei and de Lancey, 2004; Nygaard et al., 2008). The USL and CL are visceral ligaments that connect the upper vagina/cervix to the sacrum and pelvic sidewalls, respectively, and provide support to the vagina, cervix, and uterus (Ramanah et al., 2012) (Fig. 1). These ligaments are often characterized together and are commonly referred to as the USL/CL complex (Dwyer and Fattouh, 2008; Ramanah et al., 2008; Chen et al., 2013). They are, however, quite different and, for this reason, they deserve to be studied also independently. The CL is parallel to the body axis and is vertically oriented when a woman is an upright position, while the USL is dorsally directed toward the sacrum. Using an MRI based 3D technique, the CL was found to be much longer and more curved than the USL (Chen et al., 2013).

One of the first studies to investigate the existence of the CL was conducted by Mackenrodt who described the CL as a transverse cervical ligament that is the chief supporting structure of the uterus (Mackenrodt, 1895). By the 1960s, Range and Woodburne conducted an anatomical analysis of the CL, finding that it is mostly made of blood vessels, nerves, lymphatic vessels, and loose connective tissue with collagen and smooth muscle fibers (Range and Woodburne, 1964). Through a more recent structural characterization of the CL, Samaan et al. suggested the CL may be a suitable attachment point for a synthetic mesh in surgical repair of POP (Samaan et al., 2014). The CL has also been found to play a pivotal role in the treatment of cervical cancer via radical hysterectomy. Historically, the CL and its surrounding connective tissue were removed in radical hysterectomy, following a procedure that was established by Latzko and Shiffmann (1919) and Okabayashi (1921). However, studies conducted by Yabuki et al. in the 1990s and 2000s determined that preservation of the CL is crucial in order to prevent neurogenic bladder and excessive bleeding, given the proximity of the CL to the neural pathway responsible for the control of bladder function (Yabuki et al., 1991, 1996, 2005).

Investigating the effect of repeated constant loading on the time-dependent mechanical behavior of the CL and other supportive ligaments is essential since these ligaments are constantly under tension and experience large changes in length and curvature *in vivo* (Luo et al., 2014). Recently, Chen et al. used geometrical data collected via an MRI based 3D technique and developed a four-cable mechanical model in order to quantify the geometrical and mechanical characteristics of CL and USL in living healthy women (Chen et al., 2013). After reconstructing the pelvic anatomy of 20 healthy women, the authors

deduced that the CL is parallel to the body axis and, as a woman stands upright, the CL becomes vertically oriented. Due to its alignment, the CL experiences greater tension than the USL and its curvature allows the apical support to have a large range of motion. In everyday life, the CL undergoes changes in tension as a woman sits and stands upright. These changes are exacerbated with fluctuations in weight and during pregnancy when the growing fetus exerts additional tension on the pelvic organs. The CL is subjected to repeated loads over time *in vivo*, especially after the levator ani muscle is damaged during vaginal delivery. These loads are likely to cause an increase in the tissue's length over time, compromising the support function of the CL and contributing to the development of POP.

In a recent review article, we summarized the current knowledge of the mechanical properties of female reproductive organs and supporting connective tissues, presenting the results of experimental studies that characterized the nonlinear elastic and viscoelastic responses of these tissues (Baah-Dwomoh et al., 2016). *Ex vivo* uniaxial tensile tests of supportive ligaments were conducted (Reay Jones et al., 2003; Moalli et al., 2005; Vardy et al., 2005; Martins et al., 2013; Rivaux et al., 2013; Chantereau et al., 2014) and mechanical quantities, such as the ultimate strength and tensile modulus were reported for the CL (Tan et al., 2015). *In vivo* uniaxial tests were also performed to measure stiffness and repeated force-relaxation of USL/CL complexes in women affected by POP (Smith et al., 2013; Luo et al., 2014). Clearly, the *in vivo* tests produced the most physiologically relevant mechanical data but, due to ethical considerations and limited time in the operating room during testing, the tests only lasted a few minutes. Both the USL and CL are membrane-like and experience loads in multiple directions over long time intervals and thus *ex vivo* planar biaxial tests can offer a more complete description of their mechanical behavior. Using *ex vivo* planar biaxial methods, more recently, the Authors characterized the elastic, stress relaxation (Becker and De Vita, 2015), and creep (Tan et al., 2016) properties of the USL/CL complex (Fig. 1).

In this study, we investigate the effects of repeated equi-biaxial loads on the mechanical properties of swine CLs. The swine is selected as an animal model due to histological similarities that exist between the CL in swine and the CL in humans (Gruber et al., 2011; Tan et al., 2015, 2016). *Ex vivo* testing is a valuable alternative method to *in vivo* testing for exploring the time dependent behavior of CL since changes in mechanical properties can be assessed over longer time intervals. More specifically, the creep properties are evaluated after three 1200 s long equi-biaxial loads are applied along the main *in vivo* loading direction of the CL and the direction perpendicular to this one. While the CL specimens are loaded, accurate strain maps are obtained using the Digital Image Correlation (DIC) method. This study extends our limited knowledge about the time-dependent mechanical behavior of the CL, providing insight into the effect of repeated loading on the supportive function of CL within the pelvic floor. The findings could suggest new treatment strategies for PFDs and cervical cancer.

2. Materials and methods

2.1. Specimen preparation

This study was conducted with the approval of the Institutional Animal Care and Use Committee (IACUC) at Virginia Tech. Four adult (3–4 year-old, approximately 450 lbs) domestic swine were obtained from a slaughterhouse (Gunnoe Sausage Co, Goode, VA). The CLs were harvested from the swine using techniques detailed in our previous study (Tan et al., 2015). They were hydrated with phosphate-buffered saline solution (PBS, pH 7.4, Fisher Scientific, USA) and then frozen at -20°C . They were thawed at room temperature and cut into approximately $3 \times 3 \text{ cm}^2$ specimens (Fig. 2(a)–(b)). A total of 24 specimens were used for mechanical testing.

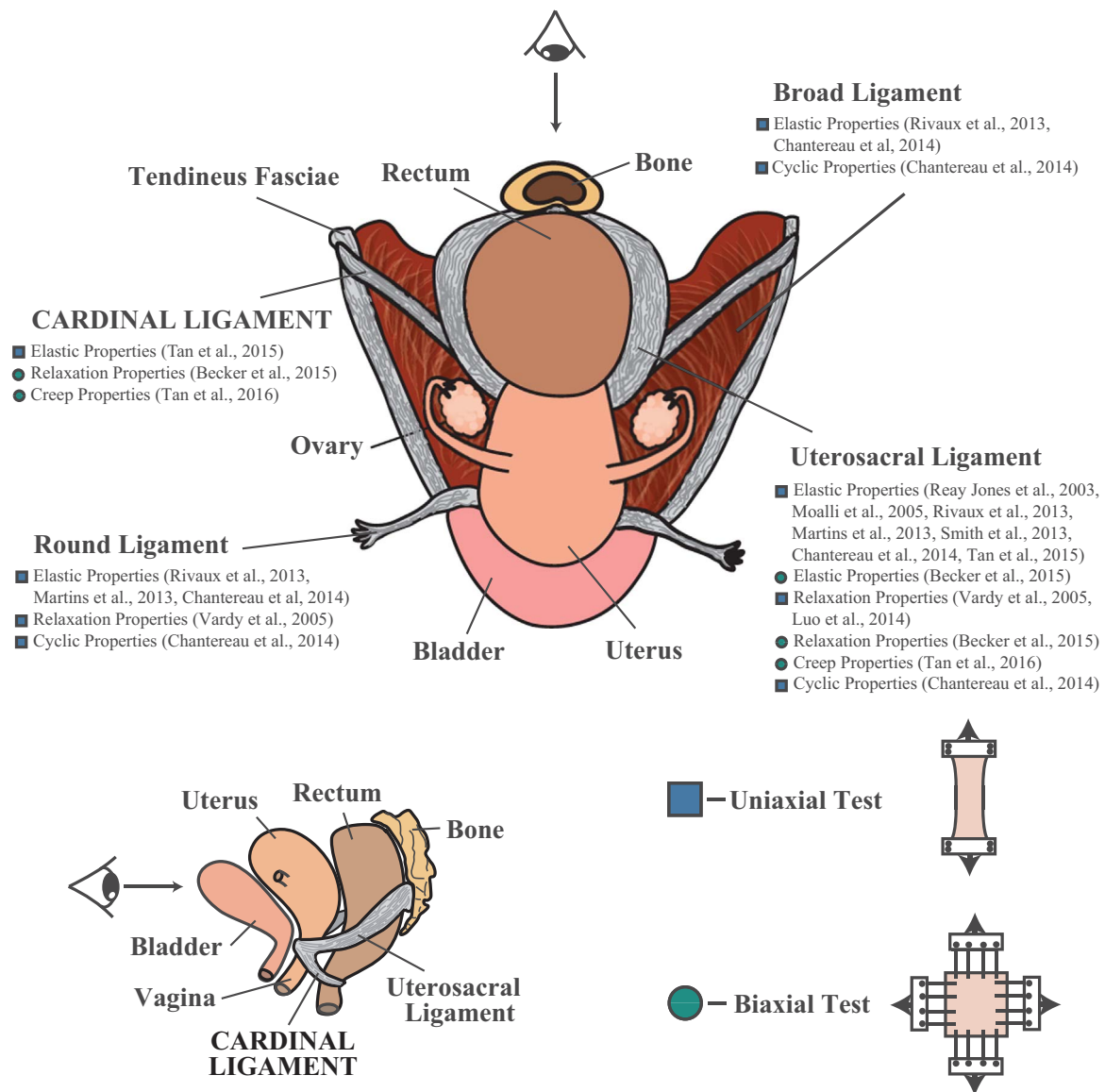


Fig. 1. Relative position of female pelvic organs and ligaments (top-down view and side view) with a list of published uniaxial and biaxial elastic and viscoelastic studies on pelvic ligaments.

2.2. Planar biaxial creep testing

Before mechanical testing, the thickness of each specimen was measured in 4 different locations using a digital caliper (accuracy ± 0.05 mm, Series 573, Mitutoyo, Japan) under a 50 g compressive load. The average thickness of each specimen was then computed and used for stress measurements. Following the methods described by Lionello et al. (2014), each specimen was immersed in a solution of PBS and methylene blue, 1% aqueous solution (Fisher Science Education, USA) and a speckle pattern was created on each specimen using an aerosol fast dry gloss white paint (McMaster-Carr, USA). Two CCD cameras (Prosilica GX 1660, Allied Vision Technologies, Exton, Pennsylvania, USA) equipped with macro lenses (AT-X 100 mm F2.8 AT-X M100 Pro D Macro Lens, Tokina, Tokyo, Japan) were employed to capture high resolution (1600×1200 pixel) images of each specimen during testing. The cameras were an integral part of the 3D digital image correlation (DIC) system (VIC-3D, Correlated Solutions, Columbia, South Carolina, USA) that was used to perform non-contact strain measurement. Before each test, images of a 12×9 mm² plastic grid with 4 mm spacing were taken in order to calibrate the DIC system. After calibration, each

specimen was gripped with 4 safety pins on each of the four sides and mounted into an Instron planar biaxial testing system equipped with four 20 N load cells (accuracy ± 0.02 N, Instron, UK). The two axial loading directions were selected to be the main *in vivo* loading direction of the CL and the direction perpendicular to this one (Fig. 2(a)–(b)). For each specimen, the distances between the two closest safety pins on opposite sides of the specimen were used to compute the two side lengths of the specimens using ImageJ (NIH, Bethesda, MD). Each of those lengths were then multiplied by the specimen's average thickness to determine the specimen's undeformed cross-sectional area along the main *in vivo* and perpendicular loading directions. The specimen was then placed in a bath made of acrylic glass (Perspex, UK) which was filled with PBS at room temperature (21 °C). The bath was then enclosed with a cover also made of acrylic glass. The acrylic glass cover came into complete contact with the PBS to create a flat planar surface for DIC measurements and to ensure that subtle fluid movements did not influence the measurements of the motion of the specimen.

Specimens ($n = 24$) were split into three groups, group 1, group 2, and group 3, based on their thicknesses and, consequently, magnitude of the equi-biaxial load applied during creep testing (Fig. 2(c)). The

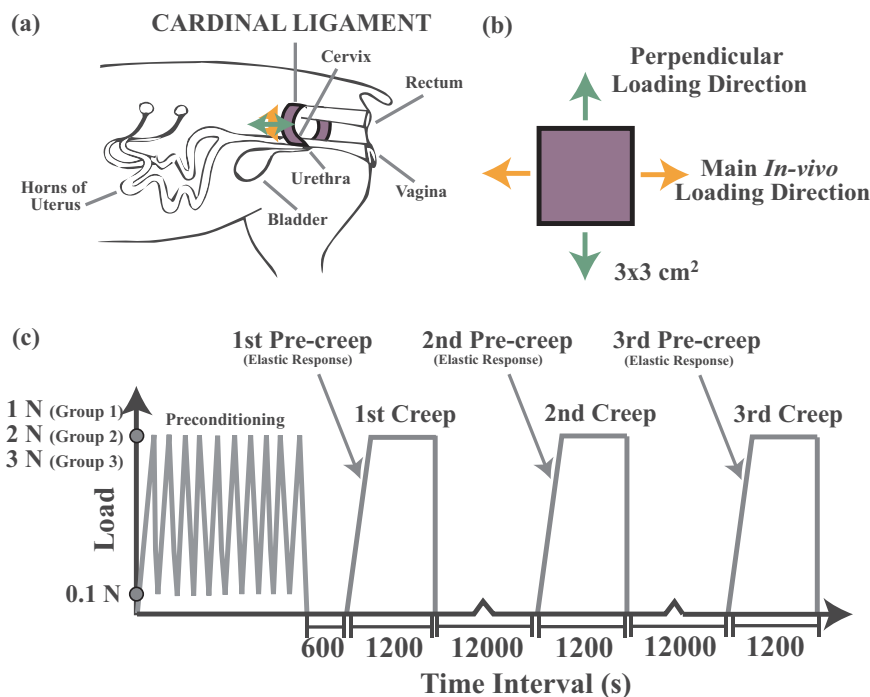


Fig. 2. (a) Location of the cardinal ligament (CL) in the swine with marked main *in vivo* (orange arrow) and perpendicular (green arrow) loading directions. (b) $3 \times 3 \text{ cm}^2$ size square specimens with sides that were oriented along the main *in vivo* (orange arrow) and perpendicular (green arrow) loading directions. (c) Load versus time protocol along each (main *in vivo* or perpendicular) axis used to test specimens at 1 N, 2 N, and 3 N equi-biaxial loads. (For interpretation of the references to color in this figure legend, the reader is referred to the web version of this article.)

specimens in each group were randomly collected from the four different swine. Thinner specimens were subjected to lower equi-biaxial loads to avoid their premature damage and failure during testing. Specimens in group 1 ($n = 8$) were preloaded to 0.1 N and preconditioned by loading/unloading them from 0.1 N to 1 N ten times at 0.05 N/s loading rate. Following preconditioning, the specimens were unloaded and allowed to recover for 600 s (= 10 min). They were then stretched at a 0.05 N/s loading rate until an equi-biaxial load of 1 N was reached. The equi-biaxial load of 1 N was held constant for 1200 s (= 20 min). Then the specimens were unloaded and allowed to recover for 12,000 s (= 200 min). The recovery time was selected to be 10 times longer than the duration of the creep test (Turner, 1973; Provenzano et al., 2002). After recovery, the specimens were again stretched at a 0.05 N/s loading rate until an equi-biaxial load of 1 N was reached. This equi-biaxial load was held constant for 1200 s (= 20 min) and then the specimens were unloaded again and allowed to recover for 12,000 s (= 200 min). Next, the specimens were stretched a final time at a 0.05 N/s loading rate until an equi-biaxial load of 1 N was reached. Again, the equi-biaxial load was held constant for 1200 s (= 20 min) and subsequently the specimens were unloaded. Specimens in group 2 ($n = 8$) and group 3 ($n = 8$) followed the same protocol but the maximum equi-biaxial loads achieved during preconditioning and held after the 600 s long recovery interval and the two 12,000 s long recovery intervals were 2 N and 3 N, respectively (Fig. 2(c)).

2.3. Data and statistical analysis

Nominal normal stress in the main *in vivo* or perpendicular loading direction was calculated by dividing the axial load (1 N, 2 N, or 3 N) in the corresponding direction by the specimen's undeformed cross-sectional area in that particular direction. This quantity will be referred simply as “stress” hereafter. Using the DIC method, the local Lagrangian strain in both axial loading directions over a square region in the center of the specimen was recorded every second for the entire duration of the test. These local axial Lagrangian strains were then averaged, resulting, at every second, in a single average Lagrangian strain value along the main *in vivo* loading direction and a single average Lagrangian strain value along the perpendicular direction. The average axial Lagrangian strain calculated for one specimen in each of the axial

directions will be further referred simply as “strain” along such direction. Figs. 3–5 show the axial Lagrangian strain map and the corresponding average values for three representative specimens at four selected times ($t = 0, 100, 600,$ and 1200 s) during the 1st creep test at 1 N, 2 N, and 3 N equi-biaxial loads, respectively. The strain (average axial Lagrangian strain) during the creep test was also normalized by dividing it, at each second, by the corresponding pre-creep strain (pre-creep average axial Lagrangian strain), that is by the strain at the beginning of the creep test. This was done for each tested specimen.

Within each specimen group (group 1, group 2, or group 3), the stress in each direction was averaged, resulting in a mean stress in the main *in vivo* loading direction and a mean stress in the perpendicular loading direction. In each specimen group, the strains along both loading directions were also averaged resulting in a mean strain in the main *in vivo* loading direction and a mean strain in the perpendicular loading direction. Next, the normalized strains in both loading directions were also analyzed at every 50 s for the entire duration (1200 s) of each creep test, that is at twenty-five time points: 0, 50, 100, 150, ..., 1200 s. A Grubb's test with $\alpha = 0.1$ was utilized to remove outliers in each specimen group based on these normalized strains. Specifically, a specimen was considered to be an outlier amongst its group if it was an outlier for over half of the twenty-five time points. By applying this test, one specimen from group 1 and one from group 3 were excluded. A Tukey's HSD test using $\alpha = 0.1$ for statistical significance was performed to compare the pre-creep strains (strains at the beginning of the creep test, that is at $t = 0 \text{ s}$) and peak strains (strains at the end of the creep test, that is at $t = 1200 \text{ s}$) between the two loading directions at each creep test (1st, 2nd, or 3rd creep test) and at each equi-biaxial load (1 N, 2 N, or 3 N equi-biaxial load). The same test was employed to compare the normalized strains at $t = 100, 600,$ and 1200 s between the two loading directions (main *in vivo* and perpendicular loading directions) at each creep test (1st, 2nd, or 3rd creep test) and at each equi-biaxial load (1 N, 2 N, or 3 N equi-biaxial load), *b*) among creep tests (1st, 2nd, and 3rd creep tests) at each equi-biaxial load (1 N, 2 N, or 3 N equi-biaxial load) and at each loading direction (main *in vivo* or perpendicular loading direction). Isochronal mean stress-strain data along the main *in vivo* and perpendicular loading directions were computed from the 1st, 2nd, and 3rd creep tests. This was done by taking the mean strains during the 1st, 2nd, and 3rd creep tests at $t = 0, 100, 600,$

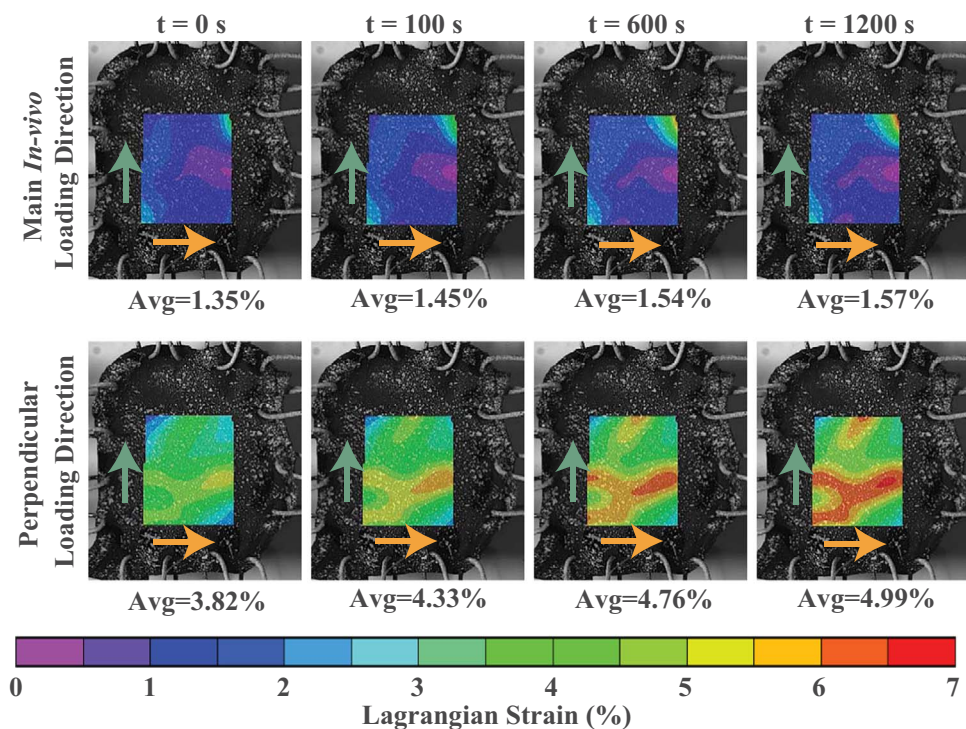


Fig. 3. Local Lagrangian strain map and corresponding average (avg) Lagrangian strain in the main *in vivo* and perpendicular loading directions at t = 0, 100, 600, and 1200 s during the 1st creep test of a representative specimen subjected to a constant 1 N equi-biaxial load. The main *in vivo* and perpendicular loading directions are denoted with orange and green arrows, respectively. (For interpretation of the references to color in this figure legend, the reader is referred to the web version of this article).

and 1200 s and their corresponding constant mean stresses for each specimen group. All data were analyzed using Minitab statistical software (Minitab 17, Minitab Inc.). Mean stresses, strains, and normalized strains in loading directions were reported together with the standard error of the mean (S.E.M.).

3. Results

3.1. Specimen group 1: Pre-creep and creep tests at 1 N equi-biaxial load

The mean stresses for specimens in group 1 ($n = 7$) subjected to creep tests at 1 N equi-biaxial load were found to be 0.0686 MPa and 0.0648 MPa in the main *in vivo* and perpendicular loading directions, respectively (Table 1). The mean pre-creep strain (i.e. the mean strain at the beginning of the 1st, 2nd or 3rd creep test) in the main *in vivo* loading direction was always lower than the mean pre-creep strain in

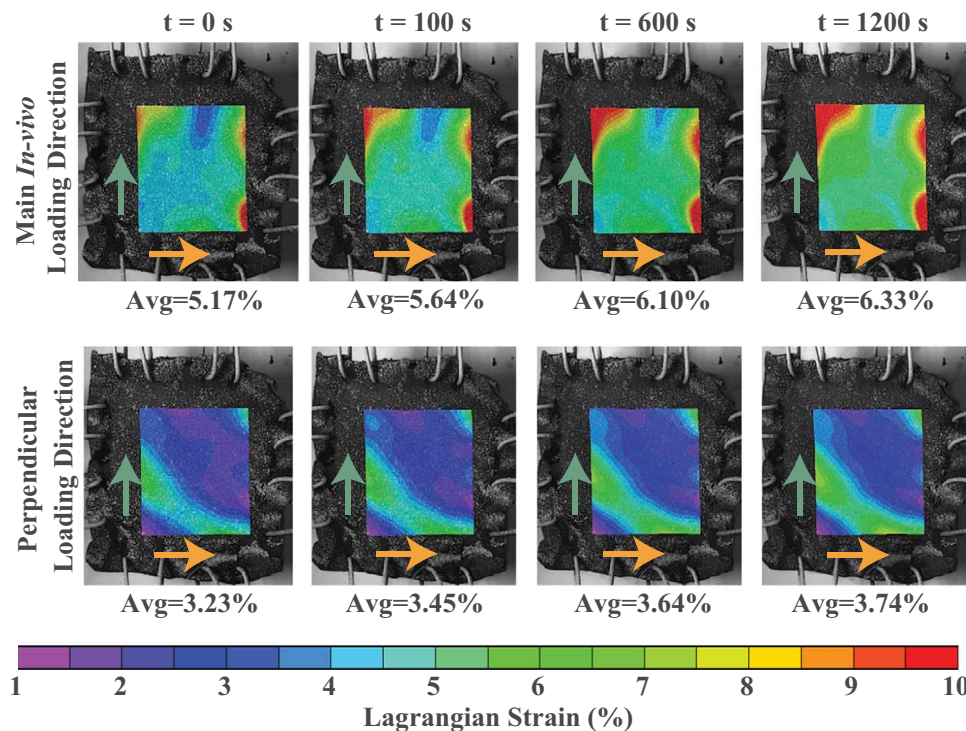


Fig. 4. Local Lagrangian strain map and corresponding average (avg) Lagrangian strain in the main *in vivo* and perpendicular loading directions at t = 0, 100, 600, and 1200 s during the 1st creep test of a representative specimen subjected to a constant 2 N equi-biaxial load. The main *in vivo* and perpendicular loading directions are denoted with orange and green arrows, respectively. (For interpretation of the references to color in this figure legend, the reader is referred to the web version of this article).

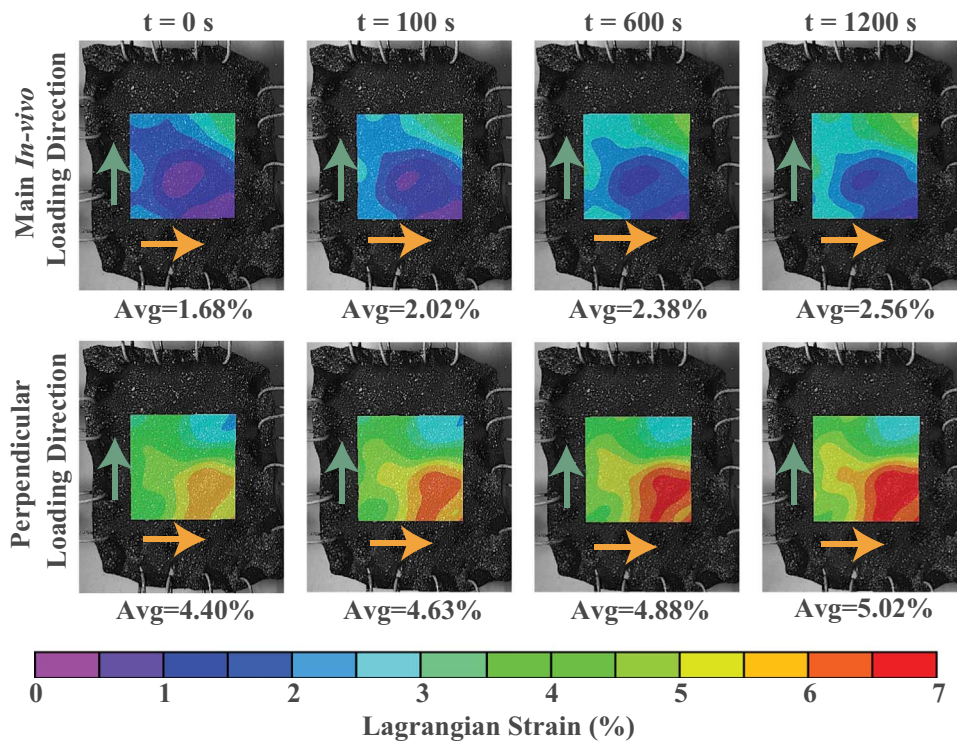


Fig. 5. Local Lagrangian strain map and corresponding average (avg) Lagrangian strain in the main *in vivo* and perpendicular loading directions at $t = 0, 100, 600,$ and 1200 s during the 1st creep test of a representative specimen subjected to a constant 3 N equi-biaxial load. Main *in vivo* and perpendicular loading directions are denoted with orange and green arrows, respectively. (For interpretation of the references to color in this figure legend, the reader is referred to the web version of this article).

Table 1
Creep test parameters for group 1 specimens ($n = 7, 1$ N equi-biaxial load, thickness: 0.51 ± 0.07 mm, mean \pm S.D.).

Mechanical quantity	Creep order	Loading direction	Value (Mean \pm S.E.M.)
Stress (MPa)		Main <i>In vivo</i>	0.0686 ± 0.004
		Perpendicular	0.0648 ± 0.003
Pre-creep strain (%)	1st	Main <i>In vivo</i>	2.738 ± 0.757
		Perpendicular	4.909 ± 0.726
	2nd	Main <i>In vivo</i>	2.283 ± 0.522
		Perpendicular	5.701 ± 1.099
	3rd	Main <i>In vivo</i>	2.351 ± 0.586
		Perpendicular	5.372 ± 0.843

the perpendicular loading direction for the 1st, 2nd or 3rd creep tests ($0.018 \leq p \leq 0.079$) (Table 1). The mean strain over time remained always lower in the main *in vivo* loading direction compared to the perpendicular loading direction (Fig. 6(a)). However, for two specimens the strain was higher along the main *in vivo* loading direction during the 1st creep test and for another specimen was higher along the main *in vivo* loading direction during the 2nd creep test (Fig. 10, Appendix A). As shown in Fig. 6(a), when comparing the mean peak strains (i.e. the mean strains at the end of the creep test) between the two loading directions at the 1st, 2nd or 3rd creep test, the mean peak strain in the perpendicular loading direction was found to be always higher than the mean peak strain in the main *in vivo* loading direction ($0.016 \leq p \leq 0.077$). However, when comparing the mean peak strains among the 1st, 2nd, 3rd creep tests along the main *in vivo* loading direction or the perpendicular loading direction, no statistical differences were found ($p = 0.706$ for the main *in vivo* loading direction comparison and $p = 0.940$ for the perpendicular loading direction comparison).

The mean stress-strain data computed from specimens in group 1 during each of the three pre-creep tests are reported in Fig. 7(a). From these mean pre-creep stress-strain curves, the CL tissue appeared to be stiffer and experienced lower strain in the main *in vivo* loading direction than in the perpendicular loading direction. The corresponding mean

normalized strain vs. time data obtained during the three creep tests are shown in Fig. 7(b). The mean normalized strains at $t = 100, 600, 1200$ s between the two loading directions were found to be not statistically different during the 1st, 2nd, or 3rd creep test ($0.293 \leq p \leq 0.989$) (Fig. 7(b)).

While comparing the mean normalized strains across the three creep tests in the main *in vivo* or perpendicular loading direction, the mean normalized strain during the 1st creep test was greater than the mean normalized strain during the 2nd and 3rd creep tests at $t = 100, 600,$ and 1200 s ($0.008 \leq p \leq 0.018$). Under constant equi-biaxial loads of 1 N, the mean normalized strain at $t = 1200$ s was approximately 1.26 times greater than the mean pre-creep strain for both the main *in vivo* and perpendicular loading directions. The 2nd creep test yielded a mean normalized strain at $t = 1200$ s approximately 1.17 and 1.13 times higher than the mean pre-creep strain in the main *in vivo* and perpendicular loading directions, respectively. After the 3rd creep test, the mean normalized strain at $t = 1200$ s was approximately 1.10 and 1.09 times higher than the mean pre-creep strain in the main *in vivo* and perpendicular loading directions, respectively. Moreover, the mean normalized strains during the 2nd and 3rd creep tests along each loading direction were not significantly different at $t = 100, 600,$ and 1200 s.

3.2. Specimen group 2: Pre-creep and creep tests at 2 N equi-biaxial load

For specimens in group 2 ($n = 8$) subjected to 2 N equi-biaxial loads, the mean stresses in the main *in vivo* and perpendicular loading directions during creep were found to be 0.0924 MPa and 0.0898 MPa, respectively (Table 2). Unlike specimens in group 1, the mean pre-creep strain in the main *in vivo* loading direction was always higher, but not significantly higher, than the mean pre-creep strain in the perpendicular loading direction for each of the three creep tests (Table 2) ($0.168 \leq p \leq 0.190$). The mean strain over time continued to be higher in the main *in vivo* loading direction compared to the perpendicular loading direction (Fig. 6(b)). This was in contrast with the findings for specimens in group 1. However, for two specimens, the strain over time was higher in the perpendicular loading direction during the three creep tests (Fig. 11, Appendix A). Moreover, when comparing the mean

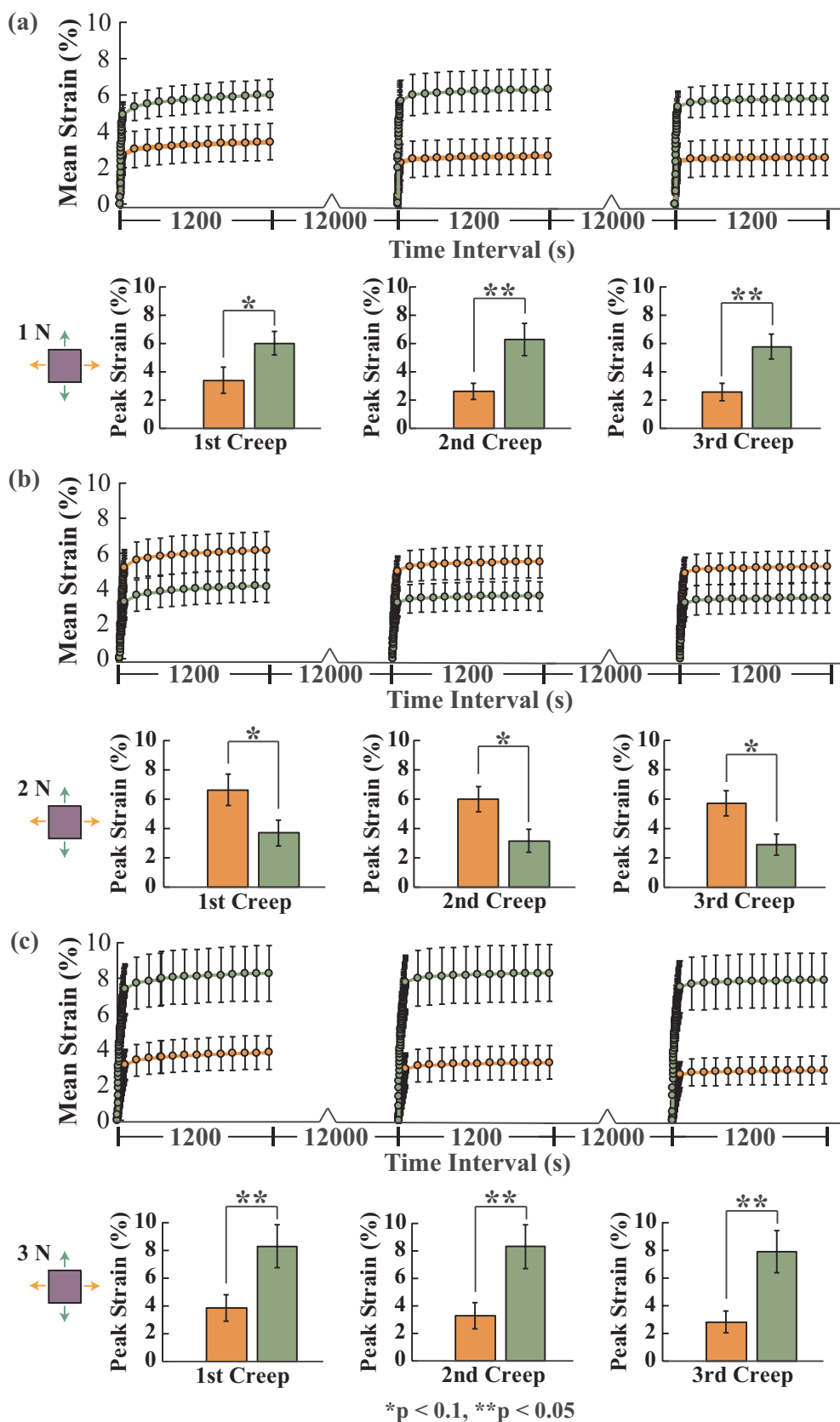


Fig. 6. Mean strain with S.E.M. vs. time curves and box plots of peak strains for (a) specimens in group 1 subjected to 1 N equi-biaxial loads during the 1st, 2nd, and 3rd creep tests ($n = 7$ specimens), (b) specimens in group 2 subjected to 2 N equi-biaxial loads during the 1st, 2nd, and 3rd creep tests ($n = 8$ specimens), and (c) specimens in group 3 subjected to 3 N equi-biaxial loads during the 1st, 2nd, and 3rd creep tests ($n = 7$ specimens). The data along the main *in vivo* and the perpendicular loading directions are reported in orange and green, respectively. Specimens experienced lower strains in the main *in vivo* loading direction at 1 N and 3 N equi-biaxial loads, but higher strains in such direction at 2 N equi-biaxial loads. (For interpretation of the references to color in this figure legend, the reader is referred to the web version of this article.)

peak strains between the two loading directions, the mean peak strain in the main *in vivo* loading direction was found to always be higher than the mean peak strain in the perpendicular loading direction for the three creep tests ($0.053 \leq p \leq 0.09$) (Fig. 6(b)). No statistical differences were noted when the mean peak strains along the main *in vivo* or

perpendicular loading direction were compared among the three creep tests at 2 N equi-biaxial loads ($p = 0.830$ for the main *in vivo* loading direction comparison and $p = 0.876$ for the perpendicular loading direction comparison).

The mean stress-strain data calculated from specimens in group 2

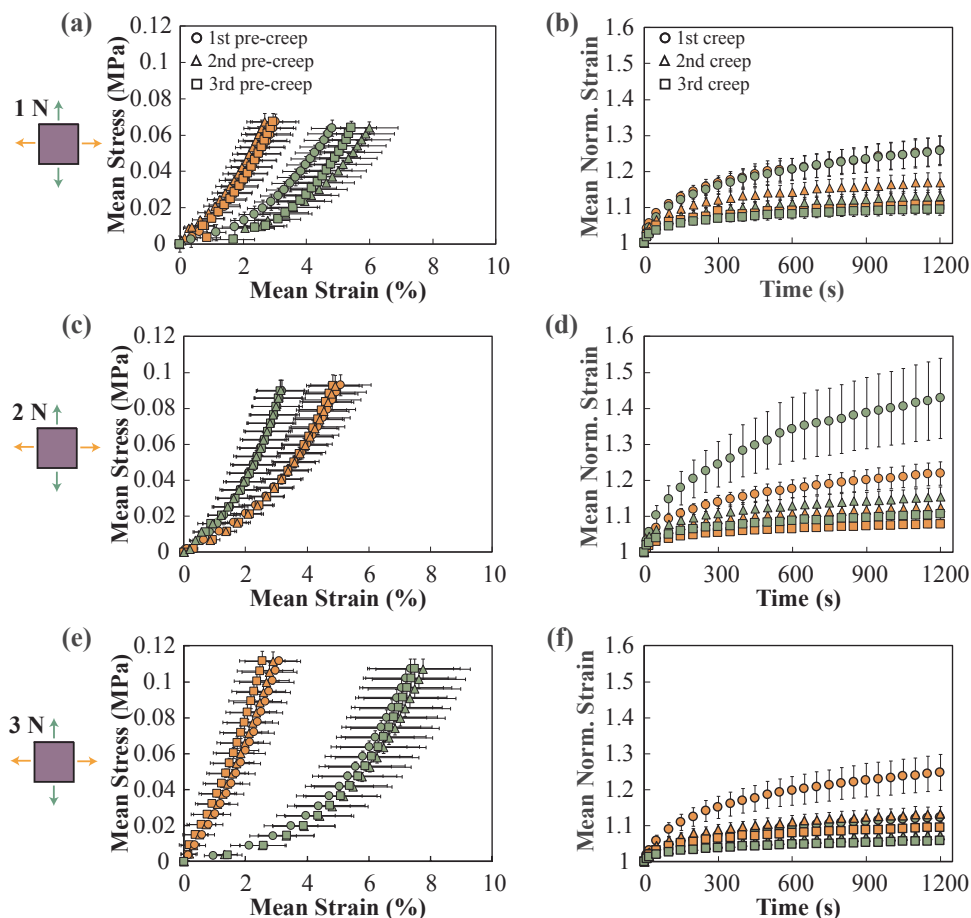


Fig. 7. Mean pre-creep stress-strain data and corresponding mean normalized strain with S.E.M. vs. time for specimens in (a)-(b) group 1 subjected to 1 N equi-biaxial loads (mean computed over $n = 7$ specimens), (c)-(d) group 2 subjected to 2 N equi-biaxial loads (mean computed over $n = 8$ specimens), and (e)-(f) group 3 subjected to 3 N equi-biaxial loads (mean computed over $n = 7$ specimens). During each pre-creep test, the CL appears to be stiffer in the main *in vivo* loading direction at 1 N and 3 N equi-biaxial loads and in the perpendicular direction at 2 N equi-biaxial loads. The mean normalized strain during the 1st creep tests at any equi-biaxial load appears to be always the greatest, regardless of loading direction.

Table 2
Creep test parameters for group 2 specimens ($n = 8$, 2 N equi-biaxial load, thickness $(0.69 \pm 0.15$ mm, mean \pm S.D.).

Mechanical quantity	Creep order	Loading direction	Value (Mean \pm S.E.M.)
Stress (MPa)		Main <i>Invivo</i>	0.0924 ± 0.005
		Perpendicular	0.0898 ± 0.006
Pre-creep strain (%)	1st	Main <i>Invivo</i>	5.213 ± 0.996
		Perpendicular	2.986 ± 0.928
	2nd	Main <i>Invivo</i>	4.999 ± 0.870
		Perpendicular	3.197 ± 0.767
	3rd	Main <i>Invivo</i>	4.894 ± 0.869
		Perpendicular	3.172 ± 0.788

before the creep tests are shown in Fig. 7(c). As the stress increased, higher strains were recorded along the main *in vivo* loading direction compared to the perpendicular loading direction during each of the pre-creep tests. The corresponding mean normalized strain vs. time data recorded during the creep tests are shown in Fig. 7(d). When comparing the mean normalized strains at $t = 100$, 600, and 1200 s as recorded during the 1st, 2nd, or 3rd creep test, no statistical differences were found between the two loading directions ($0.114 \leq p \leq 0.764$).

In each loading direction at $t = 100$ s, the mean normalized strain calculated from the 1st creep tests was not significantly different from the mean normalized strain computed from the 2nd creep tests but were greater than the mean normalized strain obtained from the 3rd creep tests ($p = 0.020$ for main *in vivo* loading direction comparison and $p = 0.046$ for perpendicular loading direction comparison). At $t = 600$ and 1200 s, the mean normalized strain calculated from the 1st creep tests was greater than both the mean normalized strains from the 2nd and

3rd creep tests ($0.002 \leq p \leq 0.005$). Thus, at constant equi-biaxial loads of 2 N, the specimens experienced always the highest increase in mean strain by the end of the 1st creep test, regardless of the loading direction. For the 1st creep tests, the mean normalized strain at $t = 1200$ s was approximately 1.22 and 1.43 times higher than the mean pre-creep strain in the main *in vivo* and perpendicular loading directions, respectively. The mean normalized strain at $t = 1200$ s for the 2nd creep tests was approximately 1.12 and 1.15 times higher than the mean pre-creep strain in the main *in vivo* and perpendicular loading directions, respectively. For the 3rd creep tests, the mean normalized strain at $t = 1200$ s was approximately 1.08 and 1.11 times higher than the mean pre-creep strain along the main *in vivo* and perpendicular loading direction, respectively. Finally, the mean normalized strains recorded during the 2nd and 3rd creep tests along the main *in vivo* or the perpendicular loading direction were not statistically different at $t = 100$, 600, and 1200 s.

3.3. Specimen group 3: Pre-creep and creep tests at 3 N equi-biaxial load

For specimens in group 3 ($n = 7$) subjected to 3 N equi-biaxial loads, the mean stresses were determined to be 0.112 MPa and 0.107 MPa in the main *in vivo* and perpendicular loading directions, respectively (Table 3). As seen for specimens in group 1, the mean pre-creep strain along the main *in vivo* loading direction was also always lower than the mean pre-creep strain in the perpendicular loading direction for the 1st, 2nd, or 3rd creep tests ($0.017 \leq p \leq 0.032$) (Table 3). Similarly, over the duration of the creep tests, the mean strain along the main *in vivo* loading direction remained lower than the mean strain along the perpendicular loading direction (Fig. 6(c)). However, for one specimen, the strain over time was higher in the main *in vivo* loading direction during the three creep tests (Fig. 12, Appendix A). As shown

Table 3
Creep test parameters for group 3 specimens ($n = 7$, 3 N equi-biaxial load, thickness: 0.98 ± 0.16 mm, mean \pm S.D.).

Mechanical quantity	Creep order	Loading direction	Value (Mean \pm S.E.M.)
Stress (MPa)		Main <i>in vivo</i>	0.112 ± 0.006
		Perpendicular	0.107 ± 0.005
Pre-creep strain (%)	1st	Main <i>in vivo</i>	3.149 ± 0.843
		Perpendicular	7.410 ± 1.400
	2nd	Main <i>in vivo</i>	2.916 ± 0.899
		Perpendicular	7.798 ± 1.537
	3rd	Main <i>in vivo</i>	2.587 ± 0.743
		Perpendicular	7.531 ± 1.478

in Fig. 6(c), the mean peak strain in the perpendicular loading direction was found to always be significantly higher than the mean peak strain in the main *in vivo* loading direction for the 1st, 2nd, or 3rd creep tests ($0.018 \leq p \leq 0.043$). Again no statistical differences in the mean peak strains among the three creep tests were noted along the main *in vivo* or perpendicular loading direction ($p = 0.766$ for the main *in vivo* loading direction comparison and $p = 0.983$ for the perpendicular loading direction comparison).

The mean stress-strain curves obtained from the data collected during the pre-creep tests for specimens in group 3 are shown in Fig. 7(e). At equal stresses, lower strains were observed along the main *in vivo* loading direction compared to the perpendicular loading direction during each of the three pre-creep tests. The corresponding mean normalized strain vs. time data recorded during the creep tests are reported in Fig. 7(f). Some statistical differences were found in the mean normalized strain between the two loading directions. For the 1st and 2nd creep test, statistical differences were found between the main *in vivo* and perpendicular loading directions at $t = 100$, 600, and 1200 s, with the mean normalized strain in the main *in vivo* loading direction being higher than the mean normalized strain in the perpendicular loading direction ($0.038 \leq p \leq 0.076$). For the 3rd creep test, the mean normalized strain was found to only be significantly different at $t = 100$ s ($p = 0.063$) between these directions and not statistically different at $t = 600$ and 1200 s ($0.107 \leq p \leq 0.112$).

In the main *in vivo* loading direction at $t = 100$ s, the mean normalized strains recorded during the 1st, 2nd, and 3rd creep tests were not statistically different ($p = 0.110$). At $t = 600$ and 1200 s, the mean normalized strain of the 1st creep was not significantly different than the mean normalized strain of the 2nd creep but was greater than the mean normalized strain of the 3rd creep ($0.028 \leq p \leq 0.038$). In the perpendicular direction at $t = 100$ s, the mean normalized strain of the 1st creep was not statistically different than the mean normalized strain of the 2nd creep but was greater than the mean normalized strain of the 3rd creep ($p = 0.012$). In this direction, at $t = 600$ and 1200 s, the mean normalized strain of the 1st creep test was significantly greater than the mean normalized strains of the 2nd and 3rd creep tests ($0.004 \leq p \leq 0.012$). Specifically, under constant 3 N equi-biaxial loads, the increase in strain during the 1st creep was always greater (although not always significantly greater) than the increase in strain during the 2nd or 3rd creep, regardless of the loading direction, as observed for specimens in group 1 and 2. During the 1st creep tests, the mean normalized strain at $t = 1200$ s was approximately 1.25 and 1.12 times higher than the mean pre-creep strain in the main *in vivo* and perpendicular loading directions, respectively. For the 2nd creep test, the mean normalized strain at $t = 1200$ s was approximately 1.13 and 1.07 times higher than the mean pre-creep strain in the main *in vivo* and perpendicular loading directions, respectively. Finally, for the 3rd creep test, the mean normalized strain at $t = 1200$ s was approximately 1.09 and 1.06 times higher than the mean pre-creep strain in the main *in vivo* and perpendicular loading directions, respectively. Along each loading direction, the mean normalized strains at $t = 100$, 600, and 1200 s for

the 2nd and 3rd creep tests were not statistically different.

3.4. Isochronal data

Isochronal mean stress-strain curves were also generated (Fig. 8). Toward this end, the stresses in the main *in vivo* loading direction and in the perpendicular loading direction were assumed to remain constant during the 1st, 2nd, and 3rd creep tests for each tested specimen. The values of these constants are reported in Tables 1–3. The mean strain values during the 1st, 2nd, and 3rd creep tests at $t = 0$, 100, 600, and 1200 s were then plotted with the corresponding constant stresses along each loading direction. The isochronal data obtained from the 1st, 2nd, and 3rd creep tests for both the main *in vivo* and perpendicular loading directions are shown in Fig. 8(a) and (b), (c) and (d), and (e) and (f), respectively. It is evident from the nonlinearities of these preliminary curves that tissues exhibited a nonlinear viscoelastic behavior.

4. Discussion

This study focuses on characterizing the mechanical behavior of the swine CL under repeated planar biaxial loads. By subjecting the ligaments to three equi-biaxial loads, the elastic and creep properties were determined in two loading directions: the main *in vivo* and perpendicular loading directions as defined in Fig. 2. The elastic response of the CL was found to be anisotropic, as in our previous study on the USL/CL complex (Becker and De Vita, 2015). On average, specimens in groups 1 and 3 were stiffer in the main *in vivo* loading direction while specimens in groups 2 were more compliant (although not significantly more compliant) in such direction (Figs. 6–7). The peak strains, which are the strains at the end of each creep test, were also different in the two loading directions for specimens in groups 1, 2, and 3. For specimens in groups 1 and 3, the mean peak strain was higher in the perpendicular direction but, for specimens in group 2, the mean peak strain was lower in such direction (Fig. 6). This anisotropy was most likely determined by the micro-structural organization of the ligament. SEM and histological analyses indicated that the collagen fibers in the CL were loosely organized, although they seemed to be primarily oriented in the main *in vivo* loading direction (Tan et al., 2015). The presence of more fibers in one loading direction could have caused the specimen to be stiffer and creep less in that direction.

Clearly, the differences in results between groups 1 and 3 and group 2 on the elastic and creep properties of the CL were determined by large inter-specimen variation as discussed in detail below but, in addition to such variation, they are likely caused by large intra-specimen variation. Fig. 9 shows three micrographs that were obtained using a confocal microscope from the same planar section of one CL. The collagen fibers within the specimen appear to have different organization, waviness, and orientation. Specifically, in Fig. 9(a), collagen fibers are oriented almost along the main *in vivo* loading direction while, in Fig. 9(b), collagen fibers are oriented along the perpendicular loading direction. Collagen fibers are also oriented perpendicular to the planar section, as cross sections of collagen fiber bundles can be detected in Fig. 9(c). Based on these preliminary images and our previous studies (Tan et al., 2016), although for several specimens the majority of the collagen fibers may have been oriented along the main *in vivo* loading direction, there may have been a large variation in the microstructure of the CL that led to conflicting results between groups 1 and 3 and group 2 as presented in Fig. 7. Specimens in group 1 and 2 did not always creep less along the main *in vivo* loading direction (Figs. 10 and 12, Appendix A) and specimens in group 2 did not always creep more in the main *in vivo* loading direction (Fig. 11, Appendix A).

The mean relative increase in strain, which was measured by the mean normalized strain, was comparable during the 1st, 2nd, or 3rd creep test in the two axial loading directions for specimens in groups 1 and 2. Some differences in mean normalized strains between the loading directions were found only for specimens in group 3 during the

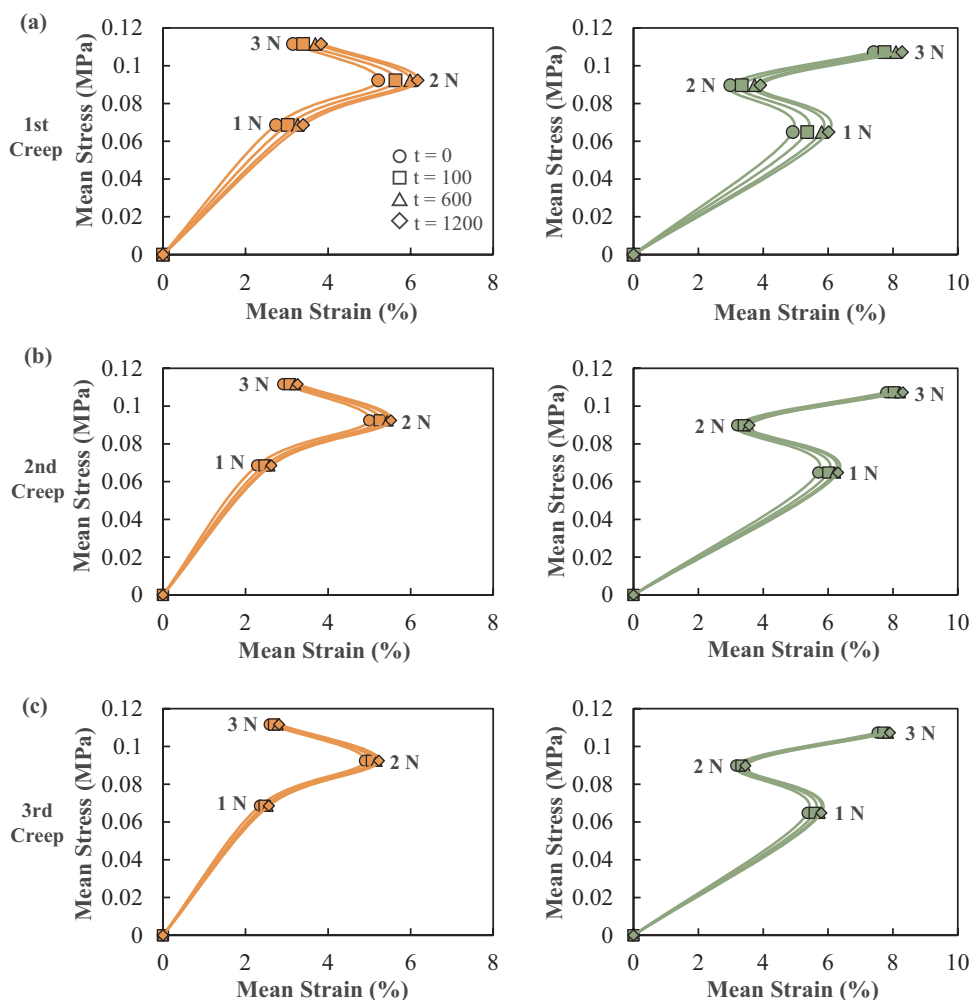


Fig. 8. Mean isochronal stress-strain curves along the main *in vivo* loading direction (orange) and perpendicular to the main *in vivo* loading direction (green) computed from stress-strain data from specimens ($n = 22$) subjected to (a) the 1st creep tests, (b) 2nd creep tests, and (c) 3rd creep tests. The nonlinearities of these curves demonstrate the non-linear creep behavior of the CL. (For interpretation of the references to color in this figure legend, the reader is referred to the web version of this article.)

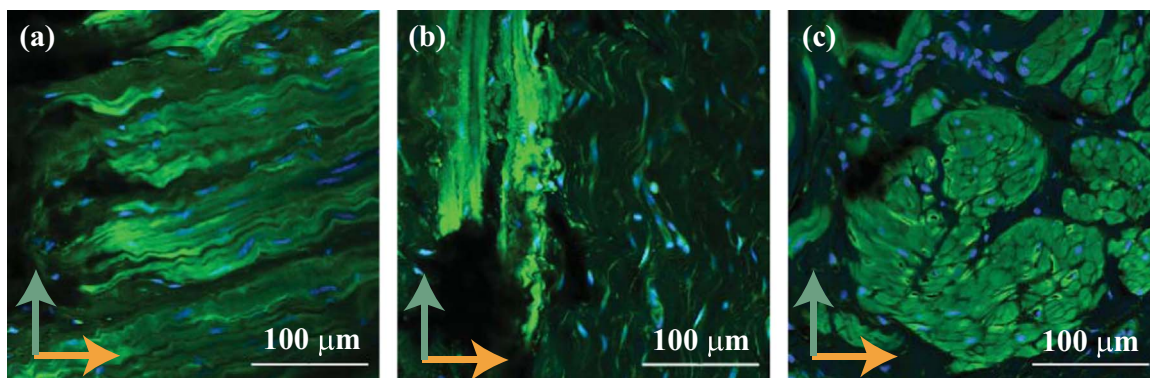


Fig. 9. Confocal microscopy images of CL stained for collagen (in green) and nuclei (in blue) taken from the planar section of one CL in three locations, clearly showing the difference in collagen alignment and orientation. Main *in vivo* and perpendicular loading directions are denoted with orange and green arrows, respectively. (For interpretation of the references to color in this figure legend, the reader is referred to the web version of this article.)

1st or 2nd creep test and at the beginning ($t = 100$ s) of the 3rd creep test. By the end of the 3rd creep test, there was no significant difference in the mean relative increase in strain between the two axial loading directions for all specimens. Other studies on relaxation and creep conducted in our lab, where the swine USL/CL complexes were subjected to single relaxation or creep tests, confirmed these findings (Becker and De Vita, 2015; Tan et al., 2016).

The mean relative increase in strain at the end (i.e., the mean normalized strain at $t = 1200$ s) of the 1st creep was always greater than the mean relative increase in strain at the end of the 3rd creep, regardless of the axial loading direction (main *in vivo* or perpendicular

loading direction) and equi-biaxial load magnitude (1 N, 2 N, or 3 N) (Fig. 7). This was likely due either to the exudation of water from the specimens or the occurrence of permanent deformation during the 1st or 2nd creep tests. When the equi-biaxial load was applied and held constant over time during the 1st or 2nd creep test, it is possible that water was forced out of the specimen. Even though the specimen was allowed to recover before the 2nd and 3rd creep tests, the water did not fully re-enter into the specimen. This decrease in water content may have reduced the relative movement of collagen fibers within the specimen, limiting the increase in strain during the 3rd creep test. This speculation is supported by a study conducted by Thornton et al. (2001)

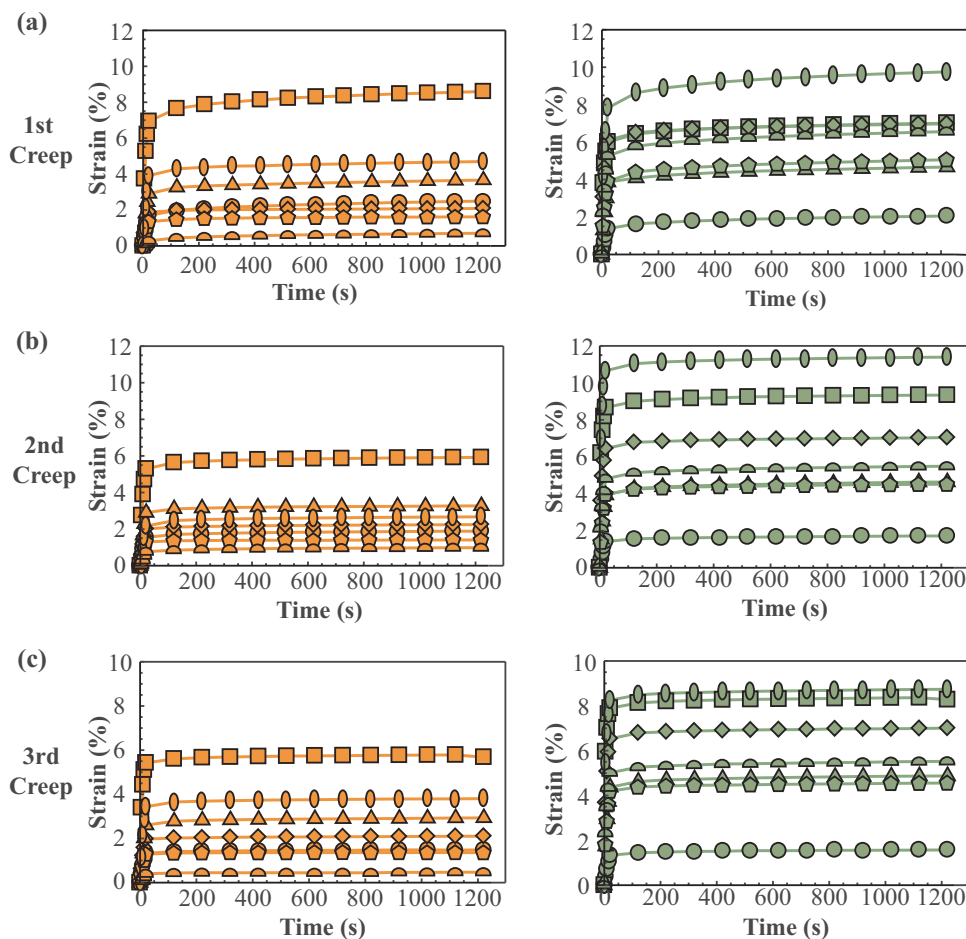


Fig. 10. Strain vs. time curves for specimens ($n = 7$) in group 1 subjected to 1 N equi-biaxial loads during the (a) 1st creep test, (b) 2nd creep test, and (c) 3rd creep test. The data for each specimen are reported using the same symbol. These symbols are orange for data collected along the main *in vivo* direction and green for data collected along the perpendicular loading direction. While specimens, on average, exhibited higher strains in the perpendicular loading direction compared to the main *in vivo* loading direction (please refer to Fig. 6(a)), this was not the case for all specimens. The specimens denoted by the circle and the square symbols exhibited higher strains in the main *in vivo* loading direction compared to the perpendicular loading direction for the 1st creep. For the 2nd creep, the specimen denoted by the circle symbols exhibited higher strains in the main *in vivo* loading direction compared to the perpendicular loading direction. (For interpretation of the references to color in this figure legend, the reader is referred to the web version of this article.)

on the effect of altering water content on the creep behavior of articular ligaments. The authors found that a decrease in hydration of these ligaments led to a decrease in creep and they deduced that a less hydrated tissue had a greater resistance to creep. In our study, we may have mechanically dehydrated the tissue during the 1st or 2nd creep test and, for this reason, we obtained results that are in agreement with those by Thornton et al. during the 3rd creep tests. In another study, Thornton et al. (2002) theorized that recruitment and straightening of the collagen fibers occurred during creep and further confirmed that collagen fiber recruitment affected the creep behavior in articular ligaments. Thus, the collagen fibers within the CL specimen may have been recruited and straightened out during the 1st or 2nd creep, inducing permanent deformation of the specimen. Once the collagen fibers were straightened, they deformed much less during the 3rd creep and, for this reason, the relative increase in strain was lower.

Overall, there was a large variability in the measured elastic and viscoelastic properties. The difference in the thickness of the specimens was a major contributing factor. Specimens were divided into three groups based on their thicknesses, with thinner specimens being tested at 1 N equi-biaxial loads and thicker specimens being tested at 2 N or 3 N equi-biaxial loads. Thicker specimens were placed in groups 2 and 3 because they had to withstand higher loads compared to thinner specimens. It must be noted that, among the three groups, specimens in group 2 exhibited the largest amount of variability with regards to specimen thickness (Table 2). This variability may have accounted for the different results between specimens in groups 1, 2, and 3 along the two axial loading directions, with specimens in group 2, unlike specimens in groups 1 and 3, experiencing higher pre-creep and peak strains in the main *in vivo* loading direction. Specimens in group 3, unlike specimens in group 1 and 2, experienced statistically different

normalized mean strains in the two axial loading directions for the 1st and 2nd creep tests. Furthermore, the large variability could be also attributed to the collection of specimens from different swine. Indeed, the swine were not fully matched with regards to age, weight, litter size, and parity. We attempted to reduce this variability by collecting as many specimens from each sow as possible and by selecting swine that were approximately the same age (3 to 4 years old) and weight (425 to 475 lbs). However, even with this large variability, some statistical differences were detected when the mean pre-creep and peak strains in the two loading directions were compared for the 1st, 2nd, or 3rd test.

One limitation of our experimental methods was the use of safety pins to clamp the specimens. Inevitably, the pins caused local stress concentration and inhomogeneities in strain. Several experimental and numerical studies investigated boundary effects due to clamping techniques on the strain and stress fields in planar biaxial testing of soft tissues (Waldman and Lee, 2002; Waldman et al., 2002; Sun et al., 2005; Eilaghi et al., 2009; Jacobs et al., 2013). According to Sun et al. (2005), using suture based gripping methods, as done in our study, for biological soft tissues reduced boundary effects. Eilaghi et al. (2009) found that the number of attachment points and the spacing of such attachment points greatly affected the strain uniformity within a specimen. In our study, we carefully attempted to place safety pins equidistantly on each side of the squared specimens. However, when working with thin, small, and soft specimens, ensuring that the safety pins were equidistant every time was impossible. It was also difficult to ensure that the safety pins were aligned along each edge of the specimen and were aligned on opposite sides of the specimen. Precautions were taken to minimize these effects, mainly by using a plastic grid as a guide to puncture the tissue with the safety pins.

After the 1st or 2nd creep test, each specimen was allowed to

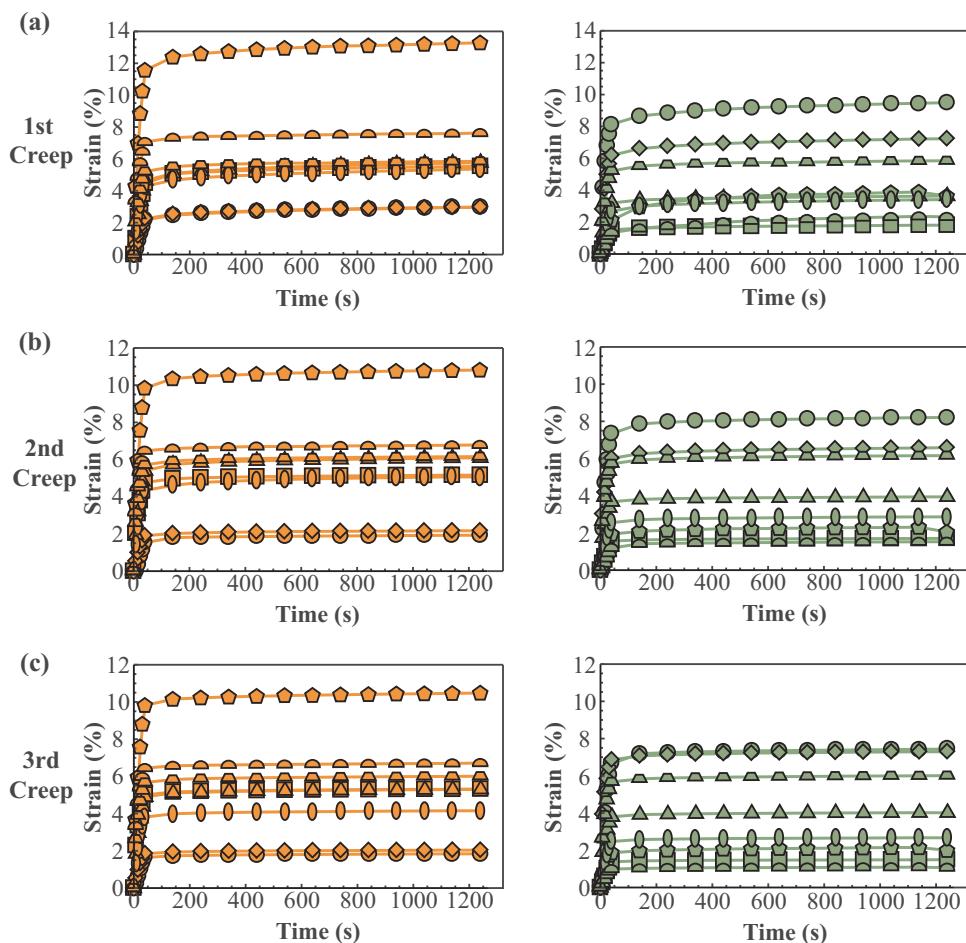


Fig. 11. Strain vs. time curves for specimens ($n = 8$) in group 2 subjected to 2 N equi-biaxial loads during the (a) 1st creep test, (b) 2nd creep test, and (c) 3rd creep test. The data for each specimen are reported using the same symbol. These symbols are orange for data collected along the main *in vivo* direction and green for data collected along the perpendicular loading direction. While specimens, on average, exhibited higher strains in the main *in vivo* loading direction compared to the perpendicular loading direction (please refer to Fig. 6(b)), this was not the case for all specimens. The specimens denoted by the circle and the diamond symbols exhibited higher strains in the perpendicular loading direction compared to the main *in vivo* loading direction for the 1st, 2nd, and 3rd creep tests. (For interpretation of the references to color in this figure legend, the reader is referred to the web version of this article.)

recover for a time interval that was ten times the time interval of the creep test, that is $1200 \times 10 \text{ s} (= 200 \text{ min})$, before subjecting the same specimen to another creep test. This recovery time was selected based on a study conducted by Turner (1973) which was, however, on nonlinear viscoelastic synthetic polymers. Realistically, we could not have increased the recovery time among creep tests since the speckle pattern created on the specimen for DIC strain measurements would not have lasted longer. Although no statistical differences in the mean peak strains among the 1st, 2nd, and 3rd creep tests, along each loading direction and for each equi-biaxial load, were found (Fig. 6), the mean normalized strain at $t = 1200 \text{ s}$ for the 1st and 3rd creep tests were statistically different. This indicated that, although the CL eventually reached comparable mean peak strain, in each loading direction and for each equi-biaxial load, it did not fully recover and thus was strained less after the 2nd recovery. Likely, the underlying microstructure of the ligament was altered during the 1st and 2nd creep tests and, as speculated above, water exudation and straightening of the collagen fibers may have occurred. No statistical differences were noted between the mean peak strains or normalized strains at $t = 0, 100, 600, 1200 \text{ s}$ along each direction during the 2nd and 3rd creep tests suggesting that, after the 2nd creep, the specimen microstructure was not altered significantly.

Isochronal stress-strain curves were generated by using only stress strain data at four time points. The nonlinearities of these curves suggested that the CL is nonlinear viscoelastic (Fig. 8). As the number of creep tests increased, the change in strain over time decreased and the mean strain at the selected four time points became more comparable for each stress. Since there was less variation in mean strain for the 2nd and 3rd creep tests compared to the 1st creep test for each specimen group, the isochronal data from the 2nd and 3rd creep tests should be

used to ascertain the nonlinear viscoelasticity of CL. More data need to be collected to draw definite conclusions on the nonlinearities of these ligaments. Ideally, in order to investigate the nonlinear viscoelasticity of these and other soft tissues, one should perform creep tests at different stress levels on the same specimens to minimize inter-specimen variability. This is, however, challenging because, as shown in this study, the 1st creep was always the highest, even when the magnitude of the subsequent equi-biaxial loads was not changed. It would also be important to determine the effect that the order of creep tests at different stress levels has on the changes in strain over time. Since no significant differences were observed between the 2nd and 3rd creep tests, one should maybe consider performing multiple creep tests at various stress levels starting from the 2nd creep.

In addition to the work published by our lab (Becker and De Vita, 2015; Tan et al., 2015, 2016), a few other studies were published on the mechanical behavior of pelvic floor ligaments (Reay Jones et al., 2003; Vardy et al., 2005; Rivaux et al., 2013; Martins et al., 2013; Chantreanu et al., 2014), as summarized in Fig. 1. Our study is, however, the first that aimed at characterizing the creep response of the CL under repeated equi-biaxial loads. Because the CL is attached to the USL at the cervix, typically both ligaments have been investigated together and have been referred to as the USL/CL complex. However, the CL is structurally and mechanically quite different from the USL (Tan et al., 2015), providing lateral support within the USL/CL complex (Chen et al., 2013; Samaan et al., 2014). In a recent anatomical study, three (distal, intermediate, proximal) sections of the CL were detected in humans, and the distal and intermediate sections were determined to be safe for surgical use as found for the USL (Buller et al., 2001; Vu et al., 2010). Together with the knowledge about the anatomy, histology, and micro-structure of the CL, a better understanding of the time dependent

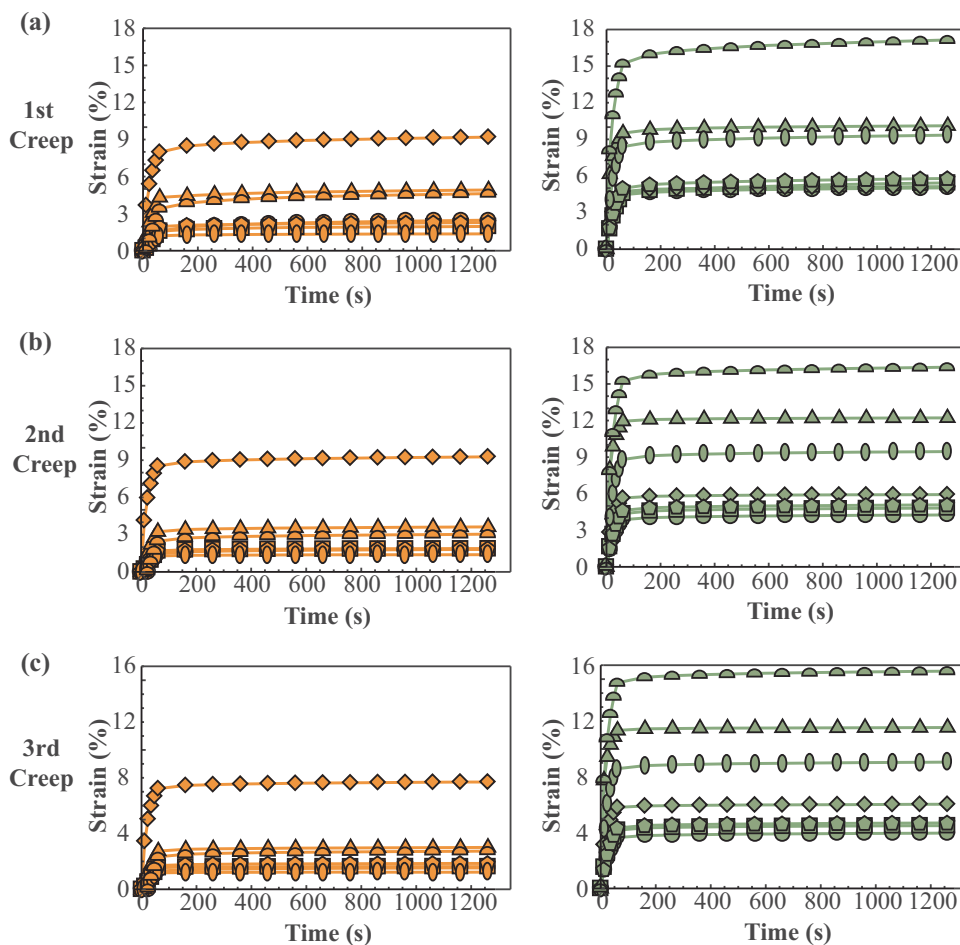


Fig. 12. Strain vs. time curves for specimens ($n = 7$) in group 3 subjected to 3 N equi-biaxial loads during the (a) 1st creep test, (b) 2nd creep test, and (c) 3rd creep test. The data for each specimen are reported using the same symbol. These symbols are orange for data collected along the main *in vivo* direction and green for data collected along the perpendicular loading direction. While specimens, on average, exhibited higher strains in the perpendicular loading direction compared to the main *in vivo* loading direction (please refer to Fig. 6(c)), this was not the case for all specimens. The specimen denoted by the diamond symbols exhibited higher strains in the main *in vivo* loading direction during the 1st, 2nd, and 3rd creep tests. (For interpretation of the references to color in this figure legend, the reader is referred to the web version of this article.)

properties of the CL can provide valuable insights into the development of effective treatment techniques for pelvic floor diseases such as POP and cervical cancer. For example, for milder cases of POP, stretching routines that control the tension/length of the ligaments and, ultimately, the support of the organs can be better designed. For invasive approaches, such as surgery, knowledge of the time-dependent properties of these ligaments may allow surgeons to establish the magnitude of the tension or to fix the length of the CL during surgical reconstruction procedures. For example, a surgeon may fix the length of the CL by taking into account the changes that will occur to this length over time under tension. In radical hysterectomy for cervical cancer, the CL is sometimes preserved since, together with its mechanical role, it offers a neural pathway to the bladder proper function. How the material behavior of CL changes with the onset of cervical cancer should be further explored to determine its role in the treatment of cervical cancer.

5. Conclusions

This experimental study presents the creep properties of the swine CL subjected to repeated equi-biaxial loads. The mean pre-creep and peak strains of the CL were found to be different in the main *in vivo* and perpendicular loading directions indicating that the collagen fibers or/and other micro-structural components are oriented differently within

Appendix A

Strain vs. time data collected during the 1st, 2nd, and 3rd creep tests for all specimens ($n = 7$) in group 1 subjected to 1 N equi-biaxial loads, all specimens ($n = 8$) in group 2 subjected to 2 N equi-biaxial loads, and all specimens ($n = 7$) in group 3 subjected to 3 N equi-biaxial loads are reported in Figs. 10, 11 and 12, respectively.

the CL specimens or respond differently to equi-biaxial loads of different magnitude. Along each loading direction, the mean peak strains resulting from the 1 N, 2 N, or 3 N equi-biaxial loads were comparable during the 1st, 2nd, and 3rd creep tests. By the end of the 3rd creep test, no statistical differences were found in the relative increase in strain over time between the main *in vivo* and perpendicular directions. Moreover, the relative increase in strain over time during the 1st creep was always the largest (although not always significantly the largest), regardless of the loading direction and load magnitude. Some nonlinearities in the viscoelastic behavior were also observed from isochronal stress-strain data. The time-dependent response of the CL and other pelvic supportive ligaments to repeated biaxial loads should be further analyzed since these ligaments are subjected to multiple constant loads *in vivo*, especially when the muscles of the pelvic floors are damaged. Effective treatment for PFDs and cervical cancer that involve the CLs can benefit from new knowledge about the viscoelasticity of these ligaments.

Acknowledgment

This material is based upon work supported by NSF PECASE Grant no. 1150397. The authors thank the Laboratory for Interdisciplinary Statistical Analysis (LISA) at Virginia Tech for helping with the statistical analysis.

References

- Baah-Dwomoh, A., McGuire, J., Tan, T., De Vita, R., 2016. Mechanical properties of female reproductive organs and supporting connective tissues: a review of the current state of knowledge. *Appl. Mech. Rev.* 68 (6), 060801.
- Becker, W.R., De Vita, R., 2015. Biaxial mechanical properties of swine uterosacral and cardinal ligaments. *Biomech. Model. Mechanobiol.* 14 (3), 549–560.
- Buller, J.L., Thompson, J.R., Cundiff, G.W., Sullivan, L.K., Ybarra, M.A.S., Bent, A.E., 2001. Uterosacral ligament: description of anatomic relationships to optimize surgical safety. *Obstet. Gynecol.* 97 (6), 873–879.
- Chantereau, P., Brieu, M., Kammal, M., Farthmann, J., Gabriel, B., Cosson, M., 2014. Mechanical properties of pelvic soft tissue of young women and impact of aging. *Int. Urogynecol. J.* 25 (11), 1547–1553.
- Chen, L., Ramanah, R., Hsu, Y., Ashton-Miller, J.A., DeLancey, J.O., 2013. Cardinal and deep uterosacral ligament lines of action: MRI based 3D technique development and preliminary findings in normal women. *Int. Urogynecol. J.* 24 (1), 37–45.
- DeLancey, J.O., 1992. Anatomical aspects of vaginal eversion after hysterectomy. *Am. J. Obstet. Gynecol.* 166 (6), 1717–1728.
- Dwyer, P.L., Fatton, B., 2008. Bilateral extraperitoneal uterosacral suspension: a new approach to correct posthysterectomy vaginal vault prolapse. *Int. Urogynecol. J.* 19 (2), 283–292.
- Eilaghi, A., Flanagan, J.G., Brodland, G.W., Ethier, C.R., 2009. Strain uniformity in biaxial specimens is highly sensitive to attachment details. *J. Biomech. Eng.* 131 (9), 091003.
- Ellington, D.R., Richter, H.E., 2013. Indications, contraindications, and complications of mesh in surgical treatment of pelvic organ prolapse. *Clin. Obstet. Gynecol.* 56 (2), 276.
- Gruber, D.D., Warner, W.B., Lombardini, E.D., Zahn, C.M., Buller, J.L., 2011. Anatomical and histological examination of the porcine vagina and supportive structures: in search of an ideal model for pelvic floor disorder. *Eval. Manag. Female Pelvic Med. Reconstr. Surg.* 17 (3), 110–114.
- Hendrix, S.L., Clark, A., Nygaard, I., Aragaki, A., Barnabei, V., McTiernan, A., 2002. Pelvic organ prolapse in the women's health initiative: gravity and gravidity. *Am. J. Obstet. Gynecol.* 186 (6), 1160–1166.
- Jacobs, N.T., Cortes, D.H., Vresilovic, E.J., Elliott, D.M., 2013. Biaxial tension of fibrous tissue: using finite element methods to address experimental challenges arising from boundary conditions and anisotropy. *J. Biomech. Eng.* 135 (2), 021004.
- Latzko, W., Shiffmann, J., 1919. Zur klinik und anatomie der erweiterten abdominalen operation des gebärmutter-krebses. *Zentralb Gynaekol* 34, 715–719.
- Lionello, G., Sirieix, C., Baleani, M., 2014. An effective procedure to create a speckle pattern on biological soft tissue for digital image correlation measurements. *J. Mech. Behav. Biomed. Mater.* 39, 1–8.
- Luo, J., Smith, T.M., Ashton-Miller, J.A., DeLancey, J.O., 2014. In vivo properties of uterine suspensory tissue in pelvic organ prolapse. *J. Biomech. Eng.* 136 (2), 021016.
- Luo, J., Betschart, C., Chen, L., Ashton-Miller, J.A., DeLancey, J.O., 2014. Using stress MRI to analyze the 3D changes in apical ligament geometry from rest to maximal valsalva: a pilot study. *Int. Urogynecology J.* 25 (2), 197–203.
- Mackenrodt, A., 1895. Ueber die ursachen der normalen und pathologischen lagen des uterus. *Arch. Gynecol. Obstet.* 48 (3), 393–421.
- MacLennan, A.H., Taylor, A.W., Wilson, D.H., Wilson, D., 2000. The prevalence of pelvic floor disorders and their relationship to gender, age, parity and mode of delivery. *BJOG: Int. J. Obstet. Gynaecol.* 107 (12), 1460–1470.
- Maher, C.M., Feiner, B., Baessler, K., Glazener, C.M., 2011. Surgical management of pelvic organ prolapse in women: the updated summary version cochrane review. *Int. Urogynecol. J.* 22 (11), 1445–1457.
- Martins, P., Silva-Filho, A.L., Fonseca, A.M., Santos, A., Santos, L., Mascarenhas, T., Jorge, R.M., Ferreira, A.M., 2013. Strength of round and uterosacral ligaments: a biomechanical study. *Arch. Gynecol. Obstet.* 287 (2), 313–318.
- Moalli, P.A., Howden, N.S., Lowder, J.L., Navarro, J., Debes, K.M., Abramowitch, S.D., Woo, S.L., 2005. A rat model to study the structural properties of the vagina and its supportive tissues. *Am. J. Obstet. Gynecol.* 192 (1), 80–88.
- Nygaard, I., Barber, M.D., Burgio, K.L., Kenton, K., Meikle, S., Schaffer, J., Spino, C., Whitehead, W.E., Wu, J., Brody, D.J., et al., 2008. Prevalence of symptomatic pelvic floor disorders in US women. *Jama* 300 (11), 1311–1316.
- Okabayashi, H., 1921. Radical abdominal hysterectomy for cancer of the cervix uteri. *Surg. Gynecol. Obstet.* 33 (4), 335–341.
- Price, D.M., Lane, F.L., Craig, J.B., Nistor, G., Motakef, S., Pham, Q.-A., Keirstead, H., 2014. The effect of age and medical comorbidities on in vitro myoblast expansion in women with and without pelvic organ prolapse. *Female Pelvic Med. Reconstr. Surg.* 20 (5), 281–286.
- Provenzano, P.P., Heisey, D., Hayashi, K., Lakes, R., Vanderby, R., 2002. Subfailure damage in ligament: a structural and cellular evaluation. *J. Appl. Physiol.* 92 (1), 362–371.
- Ramanah, R., Parratte, B., Arbez-Gindre, F., Maillet, R., Riethmuller, D., 2008. The uterosacral complex: ligament or neurovascular pathway? Anatomical and histological study of fetuses and adults. *Int. Urogynecol. J.* 19 (11), 1565–1570.
- Ramanah, R., Berger, M.B., Parratte, B.M., DeLancey, J.O., 2012. Anatomy and histology of apical support: a literature review concerning cardinal and uterosacral ligaments. *Int. Urogynecol. J.* 23 (11), 1483–1494.
- Range, R.L., Woodburne, R.T., 1964. The gross and microscopic anatomy of the transverse cervical ligament. *Am. J. Obstet. Gynecol.* 90 (4), 460–467.
- Reay Jones, N.H.J., Healy, J.C., King, L.J., Saini, S., Shousha, S., Allen-Mersh, T.G., 2003. Pelvic connective tissue resilience decreases with vaginal delivery, menopause and uterine prolapse. *Br. J. Surg.* 90 (4), 466–472.
- Rivaux, G., Rubod, C., Dedet, B., Brieu, M., Gabriel, B., Cosson, M., 2013. Comparative analysis of pelvic ligaments: a biomechanics study. *Int. Urogynecol. J.* 24 (1), 135–139.
- Samaan, A., Vu, D., Haylen, B.T., Tse, K., 2014. Cardinal ligament surgical anatomy: cardinal points at hysterectomy. *Int. Urogynecol. J.* 25 (2), 189–195.
- Smith, T.M., Luo, J., Hsu, Y., Ashton-Miller, J., DeLancey, J.O., 2013. A novel technique to measure in vivo uterine suspensory ligament stiffness. *Am. J. Obstet. Gynecol.* 209 (5) [484–e1].
- Sun, W., Sacks, M.S., Scott, M.J., 2005. Effects of boundary conditions on the estimation of the planar biaxial mechanical properties of soft tissues. *J. Biomech. Eng.* 127 (4), 709–715.
- Tan, T., Davis, F.M., Gruber, D.D., Massengill, J.C., Robertson, J.L., De Vita, R., 2015. Histo-mechanical properties of the swine cardinal and uterosacral ligaments. *J. Mech. Behav. Biomed. Mater.* 42, 129–137.
- Tan, T., Cholewa, N.M., Case, S.W., De Vita, R., 2016. Micro-structural and biaxial creep properties of the swine uterosacral-cardinal ligament complex. *Ann. Biomed. Eng.* 1–13.
- Thornton, G.M., Shrive, N.G., Frank, C.B., 2001. Altering ligament water content affects ligament pre-stress and creep behavior. *J. Orthop. Res.* 19 (5), 845–851.
- Thornton, G.M., Shrive, N.G., Frank, C.B., 2002. Ligament creep recruits fibres at low stresses and can lead to modulus-reducing fibre damage at higher creep stresses: a study in rabbit medial collateral ligament model. *J. Orthop. Res.* 20 (5), 967–974.
- Turner, S., 1973. Creep in glassy polymers. In: *The Physics of Glassy Polymers*, Springer, 1973, pp. 223–278.
- Vardy, M.D., Gardner, T.R., Cosman, F., Scotti, R.J., Mikhail, M.S., Preiss-Bloom, A.O., Williams, J.K., Cline, J.M., Lindsay, R., 2005. The effects of hormone replacement on the biomechanical properties of the uterosacral and round ligaments in the monkey model. *Am. J. Obstet. Gynecol.* 192 (5), 1741–1751.
- Vu, D., Haylen, B.T., Tse, K., Farnsworth, A., 2010. Surgical anatomy of the uterosacral ligament. *Int. Urogynecol. J.* 21 (9), 1123–1128.
- Waldman, S.D., Lee, J.M., 2002. Boundary conditions during biaxial testing of planar connective tissues. Part I: dynamic behavior. *J. Mater. Sci.: Mater. Med.* 13 (10), 933–938.
- Waldman, S., Sacks, M., Lee, J., 2002. Boundary conditions during biaxial testing of planar connective tissues. Part II: fiber orientation. *J. Mater. Sci. Lett.* 21 (15), 1215–1221.
- Wei, J.T., de Lancey, J.O., 2004. Functional anatomy of the pelvic floor and lower urinary tract. *Clin. Obstet. Gynecol.* 47 (1), 3–17.
- Wu, J.M., Hundley, A.F., Fulton, R.G., Myers, E.R., 2009. Forecasting the prevalence of pelvic floor disorders in US women: 2010–2050. *Obstet. Gynecol.* 114 (6), 1278–1283.
- Wu, J.M., Kawasaki, A., Hundley, A.F., Dieter, A.A., Myers, E.R., Sung, V.W., 2011. Predicting the number of women who will undergo incontinence and prolapse surgery, 2010–2050. *Am. J. Obstet. Gynecol.* 205 (3), 230–e1.
- Yabuki, Y., Asamoto, A., Hoshiba, T., Nishimoto, H., Kitamura, S., 1991. Dissection of the cardinal ligament in radical hysterectomy for cervical cancer with emphasis on the lateral ligament. *Am. J. Obstet. Gynecol.* 164 (1), 7–14.
- Yabuki, Y., Asamoto, A., Hoshiba, T., Nishimoto, H., Satou, N., 1996. A new proposal for radical hysterectomy. *Gynecol. Oncol.* 62 (3), 370–378.
- Yabuki, Y., Sasaki, H., Hatakeyama, N., Murakami, G., 2005. Discrepancies between classic anatomy and modern gynecologic surgery on pelvic connective tissue structure: Harmonization of those concepts by collaborative cadaver dissection. *Am. J. Obstet. Gynecol.* 193 (1), 7–15.